

Photoproduction of Jets and Heavy Flavors at Future Polarized ep - Colliders

M. Stratmann

Universität Dortmund, Institut für Physik,
D-44221 Dortmund, Germany

W. Vogelsang

Rutherford Appleton Laboratory
Chilton, Didcot, Oxon OX11 0QX, England

Abstract

We study photoproduction of jets and heavy flavors in a polarized collider mode of HERA and in polarized ep collisions at $\sqrt{S} \approx 30$ GeV. We examine the sensitivity of the cross sections and their asymmetries to the proton's polarized gluon distribution and to the completely unknown parton distributions of longitudinally polarized photons.

1 Introduction

The last few years have brought much new experimental information on the spin structure of the nucleon via measurements [1] of the spin asymmetries A_1^N ($N = p, n, d$) in longitudinally polarized deep-inelastic scattering (DIS) of leptons off polarized nucleon targets. Recent theoretical leading order (LO) [2, 3, 4] and next-to-leading order (NLO) [3, 5, 4] analyses of the data sets demonstrate, however, that these are not sufficient to accurately extract the spin-dependent quark ($\Delta q = q^\uparrow - q^\downarrow$) and gluon ($\Delta g = g^\uparrow - g^\downarrow$) densities of the nucleon. This is true in particular for $\Delta g(x, Q^2)$ since it enters DIS in LO only via the Q^2 -dependence of g_1 (or A_1) which could not yet be accurately studied experimentally. As a result of this, it turns out [3, 4] that the x -shape of Δg seems to be hardly constrained at all by the DIS data, even though a tendency towards a sizeable positive *total* gluon polarization, $\int_0^1 \Delta g(x, Q^2 = 4 \text{ GeV}^2) dx \gtrsim 1$, was found [3, 5, 4]. Clearly, the measurement of Δg is one of the most interesting challenges for future spin physics experiments.

Among the various conceivable options for future HERA upgrades is the idea to longitudinally polarize its proton beam [6] which, when combined with the already operative longitudinally polarized electron (positron) beam, results in a polarized version of the usual HERA collider with $\sqrt{S} = 298 \text{ GeV}$. A typical conservative value for the integrated luminosity in this case should be 100 pb^{-1} , but higher luminosities, up to 1000 pb^{-1} might not be inconceivable for future HERA upgrades. HERA has already been very successful in pinning down the proton's unpolarized gluon distribution $g(x, Q^2)$. Apart from exploring the unpolarized DIS structure function F_2 over a wide range in x and Q^2 [7] which indirectly constrains $g(x, Q^2)$ in global fits via scaling violations [8, 7], also processes have been studied which have contributions from $g(x, Q^2)$ already in the lowest order. Among these are (di)jet and heavy flavor production. Since events at HERA are concentrated in the region $Q^2 \rightarrow 0$, the processes have first and most accurately been studied in photoproduction [9-14]. As is well-known, in this case the (quasi-real) photon will not only interact in a direct ('point-like') way, but can also be resolved into its hadronic structure. HERA photoproduction experiments like [9-12] have not merely established evidence for the ex-

istence of such a resolved contribution, but have also been precise enough to improve our knowledge about the parton distributions, f^γ , of the photon. Here they have provided information complementary to the results for F_2^γ obtained in various e^+e^- experiments, by constraining the photonic gluon distribution [11]. More recently, the production of two jets in DIS events ($Q^2 \neq 0$) has been used for a first direct measurement of $g(x, Q^2)$ [15], and first results for the charm contribution, $F_2^c(x, Q^2)$, to F_2 have been presented [16].

Given the success of such unpolarized experiments at HERA, it seems most promising to closely examine the same processes for the situation with longitudinally polarized beams with regard to their sensitivity to Δg , which is the main purpose of this paper. Here we will focus on the *photoproduction* of open charm and jets. Firstly, as mentioned above, photoproduction experiments will yield the largest event rates and are thus expected to be more accurate. Furthermore, they may in principle allow to not only determine the parton, in particular gluon, content of the polarized *proton*, but also that of the longitudinally polarized *photon* which is completely unknown so far. Since, e.g., a measurement of the photon's spin-dependent structure function g_1^γ in polarized e^+e^- collisions is not planned in the near future, HERA could play a unique role here, even if it should only succeed in establishing the very *existence* of a resolved contribution to polarized photon-proton reactions. We emphasize at this point that the role of this contribution to photoproduction processes with polarized beams at HERA has never been investigated before: In [17] polarized photoproduction of dijets at HERA was suggested for the first time as a possible tool for measuring Δg , but the expected cross section and asymmetry were only roughly estimated, based on the single process $\gamma g \rightarrow q\bar{q}$ with the rather optimistic assumption $\Delta g/g = 0.5$, and on neglecting the resolved contribution to the cross section. Very recently, a study of open-charm photoproduction at polarized HERA was presented [18]. Again, the contribution to the cross section arising from resolved polarized photons was neglected. Even though it will turn out that for charm production this is a fairly good approximation in most cases, it clearly needs to be checked. We also believe that the issue of the sensitivity of the charm cross section to Δg was not thoroughly discussed in [18].

We note that there are also ideas for a high-luminosity polarized collider with (typ-

ically) 5 GeV electrons on 50 GeV protons at the GSI [19]. Such energies will be too low for jet physics, but are certainly appropriate for charm production. We will therefore extend our charm predictions also to this situation. As we will see, some results look more promising for lower energies since the corresponding cross section asymmetries are larger than in the HERA situation. We remark that the process $\gamma p \rightarrow c\bar{c}X$ with polarized photons and protons at (comparably low) fixed target energies has originally been suggested in the literature in [21] and further studied in [22-25]. In fact, a measurement of the spin asymmetry for the total charm photoproduction cross section is planned in a fixed target μp - experiment with $\sqrt{S} \approx 14$ GeV by the COMPASS collaboration [26]. We will essentially update and/or extend the previous studies [21-25] to the GSI ep - situation by using more up-to-date sets of polarized parton distributions covering the whole range of allowed Δg , and also by providing studies of transverse momentum and rapidity distributions of the produced charm quarks, which should be accessible with high luminosity at the GSI machine.

The paper is organized as follows: In section 2 we collect the necessary ingredients for our calculations, like the parton distributions of the proton and photon we use. Section 3 is devoted to charm production, which we study in terms of the fully inclusive charm contribution, g_1^c , to the polarized DIS structure function g_1 , but mainly as polarized open-charm photoproduction at HERA and the GSI. In section 4 we examine polarized photoproduction of (di)jets. Section 5 contains the conclusions.

2 Polarized Parton Distributions of the Proton and the Photon

As stated in the introduction, theoretical analyses of polarized DIS which take into account all or most data sets [1], have been published recently [3, 5, 4]. For the first time, these studies could even go to NLO of QCD, since the NLO framework for polarized DIS had become complete due to the calculation of the spin-dependent NLO Q^2 -evolution kernels [27]. Since, however, the NLO corrections to polarized charm or jet production are not

yet known, we have to stick to LO calculations throughout this work, which implies use of LO parton distributions¹. Fortunately, the studies [3, 4] also provide LO sets of the proton's polarized parton distributions which give an accurate description of all presently available DIS data. Both papers give various LO sets which mainly differ in the x -shape of the polarized gluon distribution, which turns out to be hardly constrained by DIS. For definiteness, we will choose the LO 'valence' set of the 'radiative parton model analysis' [3], which corresponds to the best-fit result of that paper, along with two other sets of [3] which are based on very different assumptions about the polarized gluon distribution at the low input scale μ of [3]: One set assumes $\Delta g(x, \mu^2) = g(x, \mu^2)$, which is the maximally allowed gluon input distribution obeying the fundamental positivity constraints

$$|\Delta f(x, \mu^2)| \leq f(x, \mu^2) \quad (1)$$

($f = q, g$), where the $f(x, \mu^2)$ are the unpolarized LO GRV [28] input distributions. The other set adopts $\Delta g(x, \mu^2) = 0$. It turns out that the sets A,B of [4] (GS) have gluon distributions similar to the above maximal one of [3], only the gluon of set C of [4] is qualitatively different since it has a large negative polarization at large x . We will therefore also use this set in our calculations. For illustration, we show in Fig. 1 the gluon distributions of the four different sets of parton distributions we will use, taking a typical scale $Q^2 = 10 \text{ GeV}^2$. Keeping in mind that all four sets provide very good descriptions of all present polarized DIS data [1], it becomes obvious that the data indeed do not seem to be able to significantly constrain the x -shape of $\Delta g(x, Q^2)$.

As we pointed out in the introduction, we will mainly consider photoproduction in this paper. In this case the electron just serves as a source of quasi-real photons which are radiated according to the Weizsäcker-Williams spectrum [20]. The photons can then interact either directly or via their partonic structure ('resolved' contribution). In the case of longitudinally polarized electrons, the resulting photon will be longitudinally (more precisely, circularly) polarized and, in the resolved case, the *polarized* parton distributions of the photon enter the calculations. Thus one can define the effective polarized parton

¹Note that the recent study [18] uses polarized parton distributions evolved in NLO in the LO calculation of the charm cross section for HERA. While this may sufficiently serve the purpose of numerically checking the sensitivity of the cross section to Δg , it is theoretically inconsistent since it introduces a factorization scheme dependence to the cross section.

densities at the scale M in the longitudinally polarized electron via

$$\Delta f^e(x_e, M^2) = \int_{x_e}^1 \frac{dy}{y} \Delta P_{\gamma/e}(y) \Delta f^\gamma(x_\gamma = \frac{x_e}{y}, M^2) \quad (2)$$

($f = q, g$) where $\Delta P_{\gamma/e}$ is the polarized Weizsäcker-Williams spectrum and $\Delta f^\gamma(x_\gamma, M^2)$ are the polarized photon structure functions with the additional definition $\Delta f^\gamma(x_\gamma, M^2) \equiv \delta(1 - x_\gamma)$ for the direct ('unresolved') case.

The parton distributions of polarized photons are completely unmeasured so far, such that models for the $\Delta f^\gamma(x, M^2)$ have to be invoked. In the unpolarized case, a phenomenologically very successful prediction for the unpolarized photon structure functions f^γ has emerged within the radiative parton model, where [29] a VMD valence-like structure at a low resolution scale μ was imposed as the input boundary condition, assuming that at this scale the photon entirely behaves like a vector meson, i.e., that its parton content is proportional to that of the ρ -meson. Since nothing is known experimentally about the latter, the parton densities of the neutral pion as determined in a previous study [30] were used instead which are expected not to be too dissimilar from those of the ρ . In [31, 32] a similar approach was adopted for the polarized case where, however, it is obviously impossible to uniquely fix the VMD input distributions $\Delta f^\gamma(x, \mu^2)$ in this way. Therefore, to obtain a realistic estimate for the theoretical uncertainties in the polarized photon structure functions coming from the unknown hadronic input, two very different scenarios were considered in [31, 32] with 'maximal' ($\Delta f^\gamma(x, \mu^2) = f^\gamma(x, \mu^2)$) and 'minimal' ($\Delta f^\gamma(x, \mu^2) = 0$) saturation of the fundamental positivity constraints (1). The results of these two extreme approaches are presented in Fig. 2 in terms of the photonic parton asymmetries $A_f^\gamma \equiv \Delta f^\gamma/f^\gamma$, evolved to $Q^2 = 30 \text{ GeV}^2$ in LO. An ideal aim of measurements in a polarized collider mode of HERA would of course be to determine the Δf^γ and to see which ansatz for the hadronic component is more realistic. The sets presented in Fig. 2, which we will use in what follows, should in any case be sufficient to study the sensitivity of the various cross sections to the Δf^γ , but also to see in how far they influence a determination of Δg .

We still have to specify the polarized Weizsäcker-Williams spectrum which we will use

in our calculations:

$$\Delta P_{\gamma/e}(y) = \frac{\alpha_{em}}{2\pi} \left[\frac{1 - (1-y)^2}{y} \right] \ln \frac{Q_{max}^2(1-y)}{m_e^2 y^2}, \quad (3)$$

where m_e is the electron mass. For the time being, it seems most sensible to follow as closely as possible the analyses successfully performed in the unpolarized case, which implies to introduce the same kinematical cuts. As in [10, 12, 13, 33] we will use an upper cut² $Q_{max}^2 = 4 \text{ GeV}^2$, and the y -cuts $0.2 \leq y \leq 0.85$ (for charm and single-jet [10] production) and $0.2 \leq y \leq 0.8$ (for dijet production, [12]) will be imposed. We note that a larger value for the lower limit, y_{min} , of the allowed y -interval would enhance the yield of polarized photons relative to that of unpolarized ones since $\Delta P_{\gamma/e}(y)/P_{\gamma/e}(y)$, where $P_{\gamma/e}$ is the unpolarized Weizsäcker-Williams spectrum given by

$$P_{\gamma/e}(y) = \frac{\alpha_{em}}{2\pi} \left[\frac{1 + (1-y)^2}{y} \right] \ln \frac{Q_{max}^2(1-y)}{m_e^2 y^2}, \quad (4)$$

is suppressed for small y . On the other hand, increasing y_{min} would be at the expense of reducing the individual polarized and unpolarized rates.

We finally note that in what follows a polarized cross section will always be defined as

$$\Delta\sigma \equiv \frac{1}{2} (\sigma(++) - \sigma(+-)) , \quad (5)$$

the signs denoting the helicities of the scattering particles. The corresponding unpolarized cross section is given by

$$\sigma \equiv \frac{1}{2} (\sigma(++) + \sigma(+-)) , \quad (6)$$

and the cross section asymmetry is $A \equiv \Delta\sigma/\sigma$. Whenever calculating an asymmetry A , we will use the LO GRV parton distributions for the proton [28] and the photon [29] to calculate the unpolarized cross section, which guarantees satisfaction of the positivity constraints (1). For consistency, we will employ the LO expression for the strong coupling α_s ,

$$\alpha_s(Q^2) = \frac{12\pi}{(33 - 2f) \ln(Q^2/\Lambda_{QCD}^2)}, \quad (7)$$

²In H1 analyses of HERA photoproduction data [9, 11, 14] the cut $Q_{max}^2 = 0.01 \text{ GeV}^2$ is used along with slightly different y -cuts as compared to the corresponding ZEUS measurements [10, 12, 13], which leads to smaller rates.

where f is the number of active flavors. All unpolarized [28, 29] and polarized [3, 4, 31, 32] parton distributions we employ have been set up using $\Lambda_{QCD}^{(f=4)} = 200$ MeV, which eliminates possible mismatches.

3 Charm Production at HERA and the GSI

To begin with, we study the charm contribution, g_1^c , to the spin-dependent DIS structure function g_1 . The motivation for this is that g_1^c is expected to be driven by the polarized photon-gluon fusion (PGF) subprocess³ $\gamma^* g \rightarrow c\bar{c}$. Furthermore, recently first HERA results for the unpolarized F_2^c have been reported [16], such that a measurement of g_1^c in a future high-luminosity experiment with polarized beams does not seem completely unrealistic. The results of [16] also indicate that PGF is indeed the correct mechanism for charm production. In the polarized case, its contribution to g_1 is given by [34, 23]

$$g_1^c(x, Q^2) = \frac{\alpha_s(M^2)}{9\pi} \int_{ax}^1 \frac{dy}{y} \Delta h\left(\frac{x}{y}, Q^2\right) \Delta g(y, M^2), \quad (8)$$

where

$$\Delta h(z, Q^2) = (2z - 1) \ln \frac{1 + \beta}{1 - \beta} + \beta(3 - 4z) \quad (9)$$

with $\beta^2(z) = 1 - 4m_c^2 z/Q^2(1 - z)$. In (8), $a = 1 + 4m_c^2/Q^2$ and M is some mass scale for which we will use $M = 2m_c$ (with the charm mass $m_c = 1.5$ GeV) which was shown [35] to lead to a good perturbative stability of predictions for the unpolarized F_2^c .

Fig. 3 shows our results for $g_1^c(x, Q^2)$ and the charm asymmetry $A_1^c \equiv g_1^c/F_1^c$ (with $F_1^c = (F_2^c - F_L^c)/2x$ calculated according to the unpolarized PGF process as given, e.g., in [35]) at $Q^2 = 10$ GeV² for the four different gluon distributions introduced in the last section. As becomes obvious, the results for the gluon distributions of [3] nicely reflect the relative size of the distributions in the range $x > 0.003$. However, the gluon distribution C of [4] gives a result which is rather surprising at a first glance for small values of x , the reason being the convolution of the oscillating gluon distribution (see Fig. 1) with the subprocess cross section $\Delta h(z, Q^2)$ (see eq.(9)) which also has a zero. It

³This approach implies not to treat charm as a parton of the proton which is realized in the sets of unpolarized [28] and polarized [3, 4] parton distributions we use.

becomes clear from these examples that data points at *several different* values of x would be needed in order to really pin down the shape of Δg . We note that the dashed line in Fig. 3a at $x \approx 0.005$ corresponds to about 10% of the full g_1 which implies that a fairly accurate measurement would be required. Fig. 3b also shows that the deep-inelastic charm asymmetry A_1^c is of the order of 5% or less in this x -region. It becomes much larger at larger values of x where, however, the individual g_1^c and F_1^c (or F_2^c) rapidly decrease as a result of the threshold condition $\beta^2 \geq 0$.

We now turn to the case of photoproduction of charm. For illustration, let us first consider the total cross section. In the unpolarized case it has been possible to extract the total cross section for $\gamma p \rightarrow c\bar{c}$ from the fixed target [36] and HERA [13, 14] lepton-nucleon data, i.e., the open-charm cross section for a fixed photon energy without the smearing from the Weizsäcker-Williams spectrum. To LO, the corresponding polarized cross section is given by

$$\Delta\sigma^c(S_{\gamma p}) = \sum_{f^\gamma, f^p} \int_{4m_c^2/S_{\gamma p}}^1 dx_\gamma \int_{4m_c^2/x_\gamma S_{\gamma p}}^1 dx_p \Delta f^\gamma(x_\gamma, M^2) \Delta f^p(x_p, M^2) \Delta\hat{\sigma}^c(\hat{s}, M^2). \quad (10)$$

where the Δf^p stand for the polarized parton distributions of the proton and $\hat{s} \equiv x_\gamma x_p S_{\gamma p}$. For the direct (unresolved) contribution, $\Delta f^\gamma(x_\gamma, M^2) = \delta(1 - x_\gamma)$ is to be understood. In this case, the contributing subprocess is again only PGF, $\gamma g \rightarrow c\bar{c}$, the spin-dependent total LO subprocess cross section $\Delta\hat{\sigma}^c(\hat{s})$ for which can be found in [21, 23]. In the resolved case, the processes $gg \rightarrow c\bar{c}$ and $q\bar{q} \rightarrow c\bar{c}$ contribute; their cross sections have been calculated in [37]. Needless to say that we can obtain the corresponding unpolarized LO charm cross section $\sigma^c(S_{\gamma p})$ by using LO unpolarized parton distributions and subprocess cross sections (as calculated in [38]) in (10). We note that recent HERA results for $\sigma^c(S_{\gamma p})$ are well-described by LO calculations based on the PGF process and use of standard unpolarized LO distributions such as [28].

Fig. 4 shows the result for the asymmetry $\Delta\sigma^c/\sigma^c$ for the four different sets of polarized parton distributions, where we have again used the scale $M = 2m_c$. The resolved contribution to the cross section is rather small in the unpolarized case. For the polarized case, we have calculated it using the 'maximally' saturated set for the polarized photon structure functions, which should roughly provide the maximally possible background

from resolved photons. The contribution, which was neglected in [18], turns out to be non-negligible only for large $\sqrt{S_{\gamma p}}$, where it can be as large as about 1/3 the direct contribution but with opposite sign. As becomes obvious from Fig. 4, the asymmetry becomes very small [18] towards the HERA region at larger $\sqrt{S_{\gamma p}} \sim 200$ GeV. One reason for this is the oscillation of the polarized subprocess cross section for the direct part, combined with cancellations between the direct and the resolved parts. More importantly, as seen from eq.(10), the larger $S_{\gamma p}$ becomes, the smaller are the $x_{p,\gamma}$ - values probed, such that the rapid rise of the unpolarized parton distributions strongly suppresses the asymmetry. The measurement of the *total* charm cross section asymmetry in $\gamma p \rightarrow c\bar{c}$ therefore seems rather more feasible at smaller energies, $\sqrt{S_{\gamma p}} \lesssim 20$ GeV, i.e., in the region where measurements at the GSI and in the COMPASS experiment [26] would be performed and where also the unknown resolved contribution to the cross section is negligible. Here the differences between the various gluon distributions show up rather strongly, even though measurements at various different $\sqrt{S_{\gamma p}}$ would be needed to decide between the gluons. For completeness we present in Table 1 some numbers for the total cross sections.

$\sqrt{S_{\gamma p}}$ [GeV]	fitted gluon		$\Delta g = g$ input		$\Delta g = 0$ input		GS C	
	direct [nb]	resolved [nb]	direct [nb]	resolved [nb]	direct [nb]	resolved [nb]	direct [nb]	resolved [nb]
10	10.2	-0.72	23.0	-0.63	3.46	-0.74	-3.48	-0.70
20	13.9	-0.29	23.2	0.33	3.26	-0.56	19.6	-0.70
30	9.32	0.39	13.7	1.48	1.52	-0.22	25.0	-0.35
50	2.07	1.30	1.15	2.94	-0.53	0.18	17.4	0.61
100	-4.76	2.09	-9.71	4.00	-1.90	0.46	0.58	2.27
200	-7.00	2.06	-12.8	3.60	-1.96	0.44	-8.79	3.23
300	-6.84	1.71	-12.2	2.84	-1.70	0.33	-10.4	3.21

Table 1: Total cross sections for charm photoproduction in polarized γp collisions.

From our observations for HERA-energies it follows that it could be more promising to study distributions of the cross section in the transverse momentum or the pseudorapidity of the charm quark in order to cut out the contributions from very small $x_{p,\gamma}$. We will now include the Weizsäcker-Williams spectrum since tagging of the electron, needed for

the extraction of the cross section at fixed photon energy, will probably reduce the cross section too strongly. The polarized LO cross section for producing a charm quark with transverse momentum p_T and cms-pseudorapidity η then reads

$$\frac{d^2\Delta\sigma^c}{dp_T d\eta} = 2p_T \sum_{f^e, f^p} \int_{\frac{\rho e^{-\eta}}{1-\rho e^\eta}}^1 dx_e x_e \Delta f^e(x_e, M^2) x_p \Delta f^p(x_p, M^2) \frac{1}{x_e - \rho e^{-\eta}} \frac{d\Delta\hat{\sigma}}{d\hat{t}}, \quad (11)$$

where $\rho \equiv m_T/\sqrt{S}$ with $m_T \equiv \sqrt{p_T^2 + m_c^2}$, and

$$x_p \equiv \frac{x_e \rho e^\eta}{x_e - \rho e^{-\eta}}.$$

We note that both the HERA and the GSI kinematics are asymmetric since $E_p \neq E_e$. The cross section can be transformed to the more relevant laboratory frames by a simple boost which implies

$$\eta \equiv \eta_{cms} = \eta_{LAB} - \frac{1}{2} \ln \frac{E_p}{E_e},$$

where we have, as usual, counted positive pseudorapidity in the proton forward direction. The polarized 'electronic' parton distributions $\Delta f^e(x_e, M^2)$ ($f = \gamma, q, g$) in (11) are as defined in eq.(2). The spin-dependent differential LO subprocess cross sections $d\Delta\hat{\sigma}/d\hat{t}$ for the resolved processes $gg \rightarrow c\bar{c}$ and $q\bar{q} \rightarrow c\bar{c}$ with $m_c \neq 0$ can again be found in [37]. The polarized cross section for the direct subprocess $\gamma g \rightarrow c\bar{c}$ is readily obtained from that for $gg \rightarrow c\bar{c}$ by dropping the non-abelian part and multiplying by $2N_C e_c^2 \alpha_{em}/\alpha_s$ where $e_c = 2/3$. For the factorization/renormalization scale in (11) we choose $M = m_T/2$; we will comment on the scale dependence of the results at the end of this section.

Fig. 5 shows our results for the four different sets of polarized parton distributions for the HERA case with $E_p = 820$ GeV and $E_e = 27$ GeV. Fig. 5a displays the p_T -dependence of the cross section, where we have integrated over $-1 \leq \eta_{LAB} \leq 2$. The resolved contribution to the cross section has been included, calculated with the 'maximally' saturated set of polarized photon structure functions. It is shown individually for the 'fitted Δg '-set of polarized proton distributions by the lower solid line in Fig. 5a. Comparison of the two solid lines in Fig. 5a shows that the resolved contribution is negligibly small⁴ in this case unless p_T becomes very small. The cross section in Fig. 5a should be large enough to be measurable even at $p_T \approx 15$ GeV if high luminosities can be attained. Fig.5b shows the

⁴We note that the neglect of the resolved contribution in [18] was therefore justified in this case.

asymmetries corresponding to Fig. 5a. It becomes obvious that they are much larger than for the total cross section if one goes to p_T of about 10-20 GeV, which is in agreement with the corresponding findings of [18]. Furthermore, one sees that the asymmetries are strongly sensitive to the size *and* shape of the polarized gluon distribution used. Similar statements are true for the η_{LAB} -distributions shown in Figs. 5c,d, where p_T has been integrated over $p_T > 8$ GeV in order to increase the number of events. Even here the resolved contribution remains small, although it becomes more important towards large positive values of η_{LAB} .

Fig. 6 shows similar results for the GSI situation with $E_p = 50$ GeV and $E_e = 5$ GeV. For Figs. 6a,b, η_{LAB} has been integrated over $-1 \leq \eta_{LAB} \leq 1$, and for Figs. 6c,d all events with $p_T > 3$ GeV have been collected. Again we find possibly measurable cross sections with very promising asymmetries, reaching up to about -40% for the set with the largest gluon distribution. This time, since fairly large values of x_p are probed, the negative large- x polarization of gluon C of [4] shows up prominently as an asymmetry of different sign. We note that all polarized cross sections in Figs. 5,6 are *negative* (apart from the one for GS C). This is surprising at first sight for the results at lower energy in Fig. 6 since the asymmetry for the *total* charm photoproduction cross section in Fig. 4 and Table 1 was *positive* for small $\sqrt{S_{\gamma p}}$. It turns out that the cross sections in Figs. 5,6a actually change sign at small p_T and obtain a large positive contribution from the region $p_T \lesssim m_c$ which, when integrating over p_T , compensates for the negative contribution at large- p_T shown in Figs. 5,6a. This feature once more demonstrates that in the polarized case distributions in p_T or η can be more expedient than the total cross section.

We finally briefly address the theoretical uncertainties of our results in in Figs. 5,6 related to the dependence of the cross sections and asymmetries on the renormalization/factorization scale M . Since all our calculations could be performed in LO only, this is a particularly important issue. We have therefore recalculated the results in Figs. 5,6, now using the scale $M = m_T$. As a result, it turns out that the cross sections in Fig. 5a are subject to changes of about 10% at $p_T < 15$ GeV, and of as much as 20 – 25% at larger p_T . Changes of in most cases below 10% are found for the η_{LAB} -curves in Fig. 5c.

Similar statements with generally slightly larger scale uncertainties apply to our results for lower energies in Figs. 6a,c. In contrast to this (not unexpected) fairly strong scale dependence of the polarized cross sections, the *asymmetries*, which will be the quantities actually measured, are very insensitive to scale changes, deviating usually by not more than a few percent from the values shown in Figs. 5,6 b,d for all relevant p_T and η_{LAB} . This finding seems important in two respects: Firstly, it warrants the genuine sensitivity of the asymmetry to Δg , implying that despite the sizeable scale dependence of the cross section it still seems a reasonable and safe procedure to compare LO theoretical predictions for the asymmetry with future data and to extract Δg from such a comparison. Secondly, it sheds light on the possible role of NLO corrections to our results, suggesting that such corrections might be sizeable for the cross sections, but less important for the asymmetry. This conjecture can only be confirmed or disproved once the NLO corrections to the polarized charm cross sections are known, which would be desirable for the future. We note, however, that previous experience with the spin asymmetry for prompt-photon production in hadronic collisions and the NLO corrections to it [39] supports this view.

4 Photoproduction of Jets at HERA

In this section we study photoproduction of jets. We restrict ourselves to the HERA situation since the energy of the GSI-collider would probably not be sufficient for jet physics.

The generic cross section formula for the production of a single jet with transverse momentum p_T and rapidity η is similar to that in (11), the sum now running over all properly symmetrized $2 \rightarrow 2$ subprocesses for the direct ($\gamma b \rightarrow cd$) and resolved ($ab \rightarrow cd$) cases. When only light flavors are involved one uses $m_c = 0$ in (11), and the corresponding differential helicity-dependent LO subprocess cross sections can be found in [40]. A sensible way of estimating the contribution to the cross section coming from charm quarks would be to use the (properly symmetrized) matrix elements of [37, 38] already employed for Figs. 5,6 in the previous section, which fully take into account the charm mass and

threshold effects. We found that for the values of p_T we consider in the following the effects of the finite charm mass can be safely neglected due to $m_c^2/\hat{s} \ll 1$, such that in all following predictions we will deal with the charm contribution to the cross section by including charm as a massless *final* state particle (see footnote 3) via the subprocesses $\gamma g \rightarrow c\bar{c}$ (for the direct part) and $gg \rightarrow c\bar{c}$, $q\bar{q} \rightarrow c\bar{c}$ (for the resolved part). In all following applications we will use the renormalization/factorization scale $M = p_T$. We have again found that the scale dependence of the asymmetries is rather weak as compared to that of the cross sections.

Fig. 7 shows our results for the single-inclusive jet cross section and its asymmetry as a function of p_T and integrated over $-1 \leq \eta_{LAB} \leq 2$ for the four sets of the polarized proton's parton distributions. For Figs. 7a,b we have used the 'maximally' saturated set of polarized photonic parton densities, whereas Figs. 7c,d correspond to the 'minimally' saturated set. Figs. 7a,c show that the polarized cross section is quite substantial for p_T not too large, $p_T \lesssim 15$ GeV. It is obviously also very sensitive to the polarized gluon distribution of the proton. At the same time, however, the resolved contribution to the cross section strongly dominates in the small- p_T region, as can be seen from comparison of the results in Figs. 7a,c or 7b,d. Keeping in mind that the 'true' set of polarized photon structure functions may well lie somewhere between the two extreme sets we use, this implies that, unless an experimental distinction between resolved and direct contributions can be achieved, it will hardly be possible to make a clear statement about the size of Δg and/or the polarized photonic parton distributions from a measurement of the jet cross section at these values of p_T . Furthermore, as can be seen from Figs. 7b,d, the asymmetry is very small below $p_T = 15$ GeV, which is a result of the fact that the parton distributions are mainly probed at small values of x , and of the dominance of the resolved piece (with its many contributing subprocesses) also in the unpolarized case, consequently further diluting the asymmetry. As far as a clear-cut sensitivity to Δg is concerned, the situation improves at larger p_T . Here the direct contribution clearly dominates, and the asymmetries become larger. On the other hand, the polarized cross section is very small already at $p_T \approx 25$ GeV even for the set with the largest Δg .

It appears more promising to study the η_{LAB} -distribution of the cross section and the asymmetry. The reason for this is that for negative η_{LAB} the main contributions are expected to come from the region $x_\gamma \rightarrow 1$ and thus mostly from the direct piece at $x_\gamma = 1$. To investigate this, Fig. 8 repeats the analysis presented in Fig. 7, but now as a function of η_{LAB} with p_T integrated over $p_T > 8$ GeV. Comparison of Figs. 8a,c or 8b,d (which differ in the polarized photon structure functions used) shows that indeed the direct contribution clearly dominates for $\eta_{LAB} \leq -0.5$, where also differences between the polarized gluon distributions of the proton show up clearly. Furthermore, the cross sections are generally large in this region with asymmetries of a few percents. At positive η_{LAB} , we find the same picture as for the p_T -dependence of the cross section in Fig. 7 at small p_T : The cross section is dominated by the resolved contribution and is therefore sensitive to both the parton content of the polarized proton *and* the photon. It turns out that the dominant contributions to the resolved part at large η_{LAB} are driven by the polarized photonic *gluon* distribution Δg^γ . From these results it thus appears that a measurement of the proton's Δg should be possible from single-jet events at negative rapidities where the contamination from the resolved contribution is minimal. On the other hand, one can only learn something about the polarized photon structure functions if the polarized parton distributions of the proton are already known to some accuracy.

In the unpolarized case, an experimental criterion for a distinction between direct and resolved contributions has been introduced [41] and used [12] in the case of dijet photoproduction at HERA. We will now adopt this criterion for the polarized case to see whether it would enable a better access to Δg and/or the polarized photon structure functions. The generic expression for the polarized cross section for the photoproduction of two jets with laboratory system rapidities η_1, η_2 is to LO

$$\frac{d^3 \Delta \sigma}{dp_T d\eta_1 d\eta_2} = 2p_T \sum_{f^e, f^p} x_e \Delta f^e(x_e, M^2) x_p \Delta f^p(x_p, M^2) \frac{d\Delta \hat{\sigma}}{d\hat{t}}, \quad (12)$$

where p_T is the transverse momentum of one of the two jets (which balance each other in LO) and

$$x_e \equiv \frac{p_T}{2E_e} (e^{-\eta_1} + e^{-\eta_2}),$$

$$x_p \equiv \frac{p_T}{2E_p} (e^{\eta_1} + e^{\eta_2}) . \quad (13)$$

Following [12], we will integrate over the cross section to obtain $d\Delta\sigma/d\bar{\eta}$, where $\bar{\eta} \equiv (\eta_1 + \eta_2)/2$. Furthermore, we will apply the cuts [12]

$$|\Delta\eta| \equiv |\eta_1 - \eta_2| \leq 0.5 , \quad p_T > 6 \text{ GeV} .$$

The important point is that measurement of the jet rapidities allows for fully reconstructing the kinematics of the underlying hard subprocess and thus for determining the variable [12]

$$x_\gamma^{OBS} = \frac{\sum_{jets} p_T^{jet} e^{-\eta^{jet}}}{2yE_e} , \quad (14)$$

which in LO equals $x_\gamma = x_e/y$ with y as before being the fraction of the electron's energy taken by the photon. Thus it becomes possible to experimentally select events at large x_γ , $x_\gamma > 0.75$ [41, 12], hereby extracting the *direct* contribution to the cross section with just a rather small contamination from resolved processes. Conversely, the events with $x_\gamma \leq 0.75$ will represent the resolved part of the cross section. This procedure should therefore be ideal to extract Δg on the one hand, and examine the polarized photon structure functions on the other.

Fig. 9 shows the results for the direct part of the cross section according to the above selection criteria. The contributions from the resolved subprocesses have been included, using the 'maximally' saturated set of polarized photonic parton densities. They turn out to be non-negligible but, as expected, subdominant. More importantly, due to the constraint $x_\gamma > 0.75$ they are determined by the polarized quark, in particular the u -quark, distributions in the photon, which at large x_γ are equal to their unpolarized counterparts as a result of the Q^2 -evolution (see Fig. 2), rather *independent* of the hadronic input chosen⁵. Thus the uncertainty coming from the polarized photon structure is minimal here and under control. As becomes obvious from Fig. 9, the cross sections are fairly large over the whole range of $\bar{\eta}$ displayed and very sensitive to the shape *and* the size of Δg with, however, not too sizeable asymmetries. A measurement of Δg thus could be possible under the imposed conditions. Fig. 10 displays the same results, but now for

⁵We note that the so-called LO 'asymptotic' solutions for the polarized and unpolarized photon structure functions, only valid for very large Q^2 and x , also give $A_f^\gamma \rightarrow 1$ as $x \rightarrow 1$.

the resolved contribution with $x_\gamma \leq 0.75$ for the 'maximally' saturated set (Figs. 10a,b) and the 'minimally' saturated one (Figs. 10c,d). As expected, the results depend on both the parton content of the polarized photon and the proton, which implies that the latter has to be known to some accuracy to extract some information on the polarized photon structure. It turns out that again mostly the polarized *gluon* distribution of the photon would be probed in this case, in particular at $\bar{\eta} > 0.75$. Contributions from the Δq^γ are more affected by the x_γ -cut; still such contributions amount to about 50% of the cross section at $\bar{\eta} = 0$. We finally emphasize that the experimental finding of a non-vanishing asymmetry would establish at least the definite existence of a resolved contribution to the polarized cross section.

5 Summary and Conclusions

We have analyzed various conceivable spin-physics experiments at possibly forthcoming future polarized *ep*-colliders with high luminosity at HERA and the GSI. Here we have studied the charm contribution, g_1^c , to the polarized DIS structure function g_1 and photoproduction of open charm and jets. All processes we have considered have in common that they get contributions from incoming gluons already in the lowest order and thus look promising tools to measure the polarized gluon distribution of the proton. In addition, they all have already been successfully studied in the unpolarized case at HERA which also provides a guidance concerning the experimental cuts to be used in the calculations.

The DIS charm contribution $g_1^c(x, Q^2 = 10 \text{ GeV}^2)$ turns out to be strongly dependent on the size and shape of Δg ; however, it constitutes a sizeable part of g_1 only in the region $x < 0.05$.

The photoproduction experiments we have studied derive their importance from their sensitivity not only to Δg , but also to the completely unknown parton content of the polarized photon entering via the resolved contributions to the polarized cross sections. As far as a 'clear' determination of Δg is concerned, this resolved piece, if non-negligible, might potentially act as an obstructing background, and it is therefore crucial to assess its

possible size. For this purpose, we have employed two very different sets for the polarized photonic parton distributions which are based on different assumptions concerning the hadronic (VMD) input. Conversely, and keeping in mind that HERA has been able to provide much new information on the unpolarized hadronic structure of the photon, it is also conceivable that photoproduction experiments at a polarized version of HERA could be *the* place to actually look for effects of the polarized photon structure and to prove the existence of resolved contributions to the polarized cross sections and asymmetries.

From these points of view, our main results can be summarized as follows: In the case of open-charm photoproduction we found that the resolved contribution is generally negligible except for the *total* charm cross section at HERA energies. Furthermore, the cross sections and their asymmetries are very sensitive to shape and size of Δg . This is true in particular for the distribution of the cross section in pseudorapidity, where also both cross section and asymmetry appear large enough to be measurable at HERA and/or the GSI machine with sufficient accuracy to decide between the various possible scenarios for Δg . Concerning photoproduction of jets, we find a generally much larger size of the resolved contribution. It turns out that the rapidity-distribution of the single-inclusive jet cross section separates out the direct part of the cross section at negative rapidities. In this region again a strong dependence on Δg is found with larger cross sections than for the case of charm production, but smaller asymmetries. At larger rapidities the cross section becomes sensitive to both the parton content of the polarized proton *and* photon, and an extraction of either of them does not seem straightforward. The situation improves when considering dijet production and adopting an analysis successfully performed in the unpolarized case [41, 12] which is based on reconstructing the kinematics of the underlying subprocess and thus effectively separating direct from resolved contributions. We find that in this case the (experimentally defined) direct contribution should provide access to Δg whereas the resolved part, if giving rise to a non-vanishing asymmetry, would establish existence of a polarized parton content of the photon. We finally emphasize that the corresponding measurements will not be easy since the involved asymmetries are not very large despite sizeable polarized cross sections. With expected high luminosities they seem a very interesting challenge for future polarized ep colliders at DESY or the GSI.

Acknowledgements

We are thankful to M. Glück for helpful discussions. The work of M.S. has been supported in part by the 'Bundesministerium für Bildung, Wissenschaft, Forschung und Technologie', Bonn.

References

- [1] A recent overview on the experimental status can be found, e.g., in R. Voss, in proceedings of the workshop on 'Deep Inelastic Scattering and QCD (DIS '95)', Paris, 1995, eds. J.F. Laporte and Y. Sirois.
- [2] M. Glück, E. Reya and W. Vogelsang, Phys. Lett. **B359**, 201 (1995). The LO analysis presented in this paper was updated in [3].
- [3] M. Glück, E. Reya, M. Stratmann and W. Vogelsang, Phys. Rev. **D53**, 4775 (1996).
- [4] T. Gehrmann and W.J. Stirling, Univ. of Durham report DTP/95/82, to appear in Phys. Rev. **D**.
- [5] R.D. Ball, S. Forte, and G. Ridolfi, CERN-TH/95-266, to appear in Phys. Lett. **B**.
- [6] D. Barber, in proceedings of the 'Zeuthen Workshop on the Prospects of Spin Physics at HERA', DESY 95-200, p.76, eds. J. Blümlein and W.D. Nowak.
- [7] M. Derrick et al., ZEUS collab., Z. Phys. **C69**, 607 (1996);
S. Aid et al., H1 collab., DESY 96-039.
- [8] M. Derrick et al., ZEUS collab., Phys. Lett. **B345**, 576 (1995);
S. Aid et al., H1 collab., Phys. Lett. **B354**, 494 (1995).
- [9] I. Abt et al., H1 collab., Phys. Lett. **B314**, 436 (1993).
- [10] M. Derrick et al., ZEUS collab., Phys. Lett. **B342**, 417 (1995).
- [11] T. Ahmed et al., H1 collab., Nucl. Phys. **B445**, 195 (1995).

- [12] M. Derrick et al., ZEUS collab., Phys. Lett. **B348**, 665 (1995).
- [13] M. Derrick et al., ZEUS collab, Phys. Lett. **B349**, 225 (1995).
- [14] S. Aid et al., H1 collab., DESY 96-055.
- [15] S. Aid et al., H1 collab., Nucl. Phys. **B449**, 3 (1995).
- [16] A. De Roeck, H1 collab., talk presented at the 'Cracow Epiphany Conference on the Proton Structure', Cracow, 1996, to appear in Acta Phys. Polon.
- [17] Z. Kunszt, Phys. Lett. **B218**, 243 (1989).
- [18] S. Frixione and G. Ridolfi, INFN-Genova report GEF-TH-4/1996, hep-ph 9605209.
- [19] A. Schäfer, private communication; see also <http://www.gsi.de> for information on the workshop on 'Long-Term Perspectives of GSI'.
- [20] C.F. von Weizsäcker, Z. Phys. **88**, 612 (1934);
E.J. Williams, Phys. Rev. **45**, 729 (1934).
- [21] M. Glück and E. Reya, Z. Phys. **C39**, 569 (1988).
- [22] G. Altarelli and W.J. Stirling, Particle World **1**, 40 (1989).
- [23] M. Glück, E. Reya and W. Vogelsang, Nucl. Phys. **B351**, 579 (1991).
- [24] S.I. Alekhin, V.I. Borodulin and S.F. Sultanov, Int. J. of Mod. Phys. **A8**, 1603 (1993).
- [25] S. Keller and J.F. Owens, Phys. Rev. **D49**, 1199 (1994).
- [26] G. Baum et al., COMPASS Collab., CERN/SPSLC 96-14.
- [27] R. Mertig and W.L. van Neerven, Univ. Leiden report INLO-PUB-6/95 and NIKHEF-H/95-031, to appear in Z. Phys. **C**;
W. Vogelsang, Rutherford report RAL-TR-95-071, to appear in Phys. Rev. **D**, and Rutherford report RAL-TR-96-020.
- [28] M. Glück, E. Reya, and A. Vogt, Z. Phys. **C67**, 433 (1995).

- [29] M. Glück, E. Reya, and A. Vogt, Phys. Rev. **D46**, 1973 (1992).
- [30] M. Glück, E. Reya, and A. Vogt, Z. Phys. **C53**, 651 (1992).
- [31] M. Glück and W. Vogelsang, Z. Phys. **C55**, 353 (1992), Z. Phys. **C57**, 309 (1993).
- [32] M. Glück, M. Stratmann and W. Vogelsang, Phys. Lett. **B337**, 373 (1994).
- [33] M. Klasen, G. Kramer and S.G. Salesch, Z. Phys. **C68**, 113 (1995);
M. Klasen and G. Kramer, Phys. Lett. **B366**, 385 (1996) and DESY 95-226.
- [34] A.D. Watson, Z. Phys. **C12**, 123 (1982).
- [35] M. Glück, E. Reya and M. Stratmann, Nucl. Phys. **B422**, 37 (1994).
- [36] see M. Arneodo et al., EMC, Z. Phys. **C35**, 1 (1987), and references therein.
- [37] A.P. Contogouris, S. Papadopoulos and B. Kamal, Phys. Lett. **246**, 523 (1990);
M. Karliner and R.W. Robinett, Phys. Lett. **B324**, 209 (1994).
- [38] L.M. Jones and H.W. Wyld, Phys. Rev. **D17**, 759 (1978);
M. Glück, J.F. Owens and E. Reya, Phys. Rev. **D17**, 2324 (1978);
J. Babcock, D. Sivers and S. Wolfram, Phys. Rev. **D18**, 162 (1978);
B. Combridge, Nucl. Phys. **B151**, 429 (1979).
- [39] A.P. Contogouris, B. Kamal, Z. Merebashvili and F.V. Tkachov, Phys. Lett. **B304**,
329 (1993); Phys. Rev. **D48**, 4092 (1993);
L.E. Gordon and W. Vogelsang, Phys. Rev. **D48**, 3136 (1993); **D49**, 170 (1994).
- [40] J. Babcock, E. Monsay and D. Sivers, Phys. Rev. **D19**, 1483 (1979).
- [41] J.R. Forshaw and R.G. Roberts, Phys. Lett. **B319**, 539 (1993).

Figure Captions

Fig.1 Gluon distributions at $Q^2 = 10 \text{ GeV}^2$ of the four LO sets of polarized parton distributions used in this paper. The dotted line refers to set C of [4], whereas the other distributions are taken from [3] as described in the text.

Fig.2 Photonic LO parton asymmetries $A_f^\gamma \equiv \Delta f^\gamma / f^\gamma$ at $Q^2 = 30 \text{ GeV}^2$ for the two scenarios considered in [31, 32] (see text). The unpolarized LO photonic parton distributions were taken from [29].

Fig.3 a: Charm contribution, g_1^c , to g_1 at $Q^2 = 10 \text{ GeV}^2$ for the four gluon distributions of Fig. 1, calculated according to Eq.(8) using $M = 2m_c$ and $m_c = 1.5 \text{ GeV}$. **b:** Charm asymmetry corresponding to **a**.

Fig.4 Asymmetry for the total charm photoproduction cross section vs. the photon-proton cms energy $\sqrt{S_{\gamma p}}$, calculated according to Eq.(10) using $M = 2m_c$ and $m_c = 1.5 \text{ GeV}$.

Fig.5 a: p_T -dependence of the (negative) polarized charm-photoproduction cross section in ep -collisions at HERA, calculated according to Eq.(11) (using $M = m_T/2$ and $m_c = 1.5 \text{ GeV}$) and integrated over $-1 \leq \eta_{LAB} \leq 2$. The line drawings are as in the previous figures. For comparison the resolved contribution to the cross section, calculated with the 'fitted Δg ' gluon distribution of [3] and the 'maximally' saturated set of polarized photonic parton distributions is shown by the lower solid line. **b:** Asymmetry corresponding to **a**. **c,d:** Same as **a,b**, but for the η_{LAB} dependence, integrated over $p_T > 8 \text{ GeV}$.

Fig.6 Same as Fig. 5, but for $E_p = 50 \text{ GeV}$, $E_e = 5 \text{ GeV}$ (GSI). For **a,b** we have integrated over $-1 \leq \eta_{LAB} \leq 1$ and for **c,d** over $p_T > 3 \text{ GeV}$. To avoid confusion due to the sign of the cross section, the result for set C of [4] is only shown in the asymmetry plots.

Fig.7 a: p_T -dependence of the polarized single-jet inclusive photoproduction cross section in ep -collisions at HERA, integrated over $-1 \leq \eta_{LAB} \leq 2$. The renormalization/factorization scale was chosen to be $M = p_T$. The resolved contribution to the

cross section has been calculated with the 'maximally' saturated set of polarized photonic parton distributions. Note that we show the *absolute* value of the cross sections; the respective signs can be inferred from **b**. **b**: Asymmetry corresponding to **a**. **c,d**: Same as **a,b**, but for the 'minimally' saturated set of polarized photonic parton distributions.

Fig.8 Same as Fig. 7, but for the η_{LAB} -dependence of the cross section, integrated over $p_T > 8$ GeV.

Fig.9 a: $\bar{\eta}$ -dependence of the 'direct' part of the polarized two-jet photoproduction cross section in ep -collisions at HERA for the four different sets of polarized parton distributions of the proton. The experimental criterion $x_\gamma^{OBS} > 0.75$ has been applied to define the 'direct' contribution (see text). The resolved contribution with $x_\gamma^{OBS} > 0.75$ has been included using the 'maximally' saturated set of polarized photonic parton distributions. **b**: Asymmetry corresponding to **a**.

Fig.10 Same as Fig. 9, but for the resolved part of the cross section, defined by $x_\gamma^{OBS} \leq 0.75$ (see text). For **a,b**: the 'maximally' saturated set of polarized photonic parton distributions has been used and for **c,d** the 'minimally' saturated one.

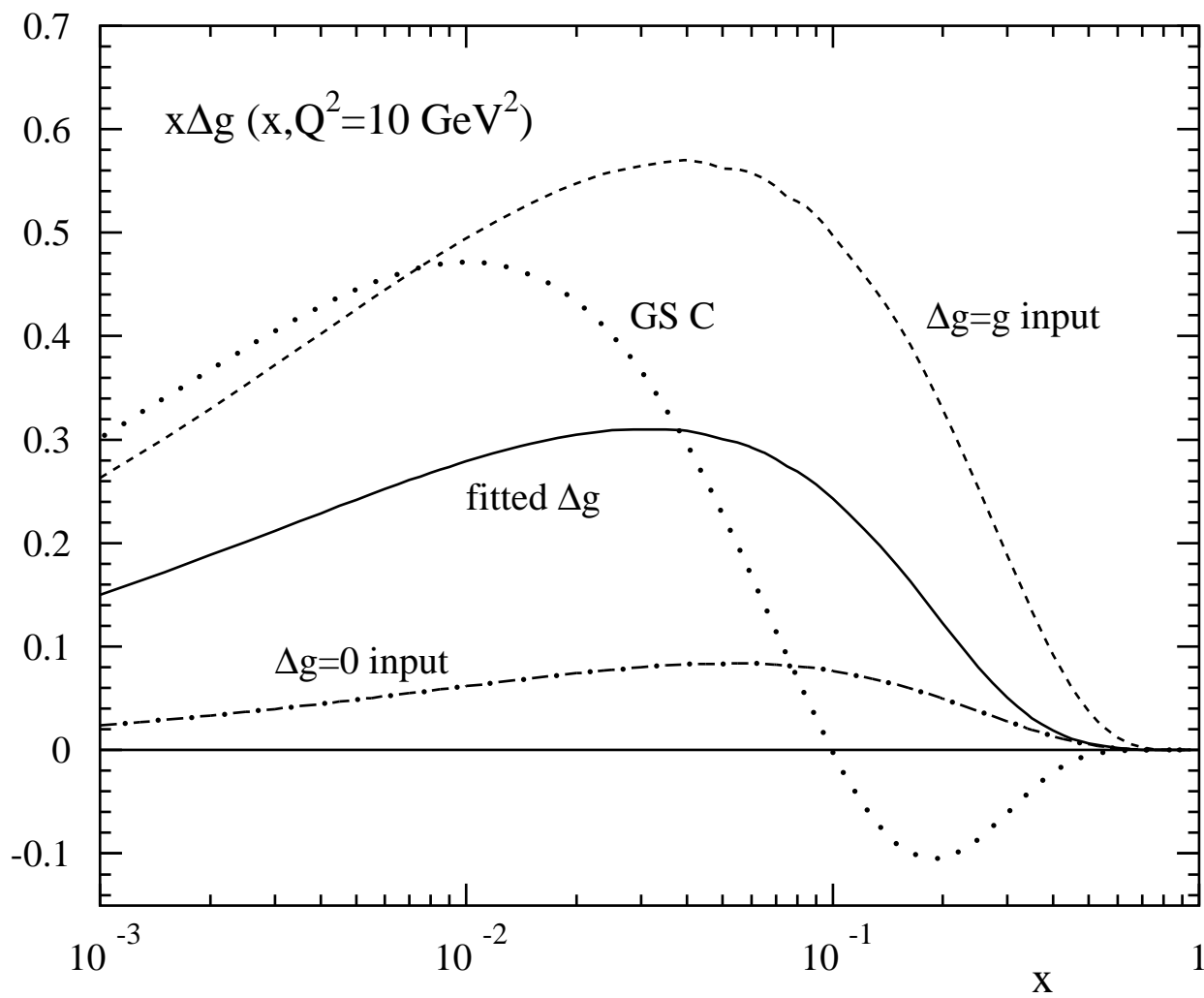


Fig. 1

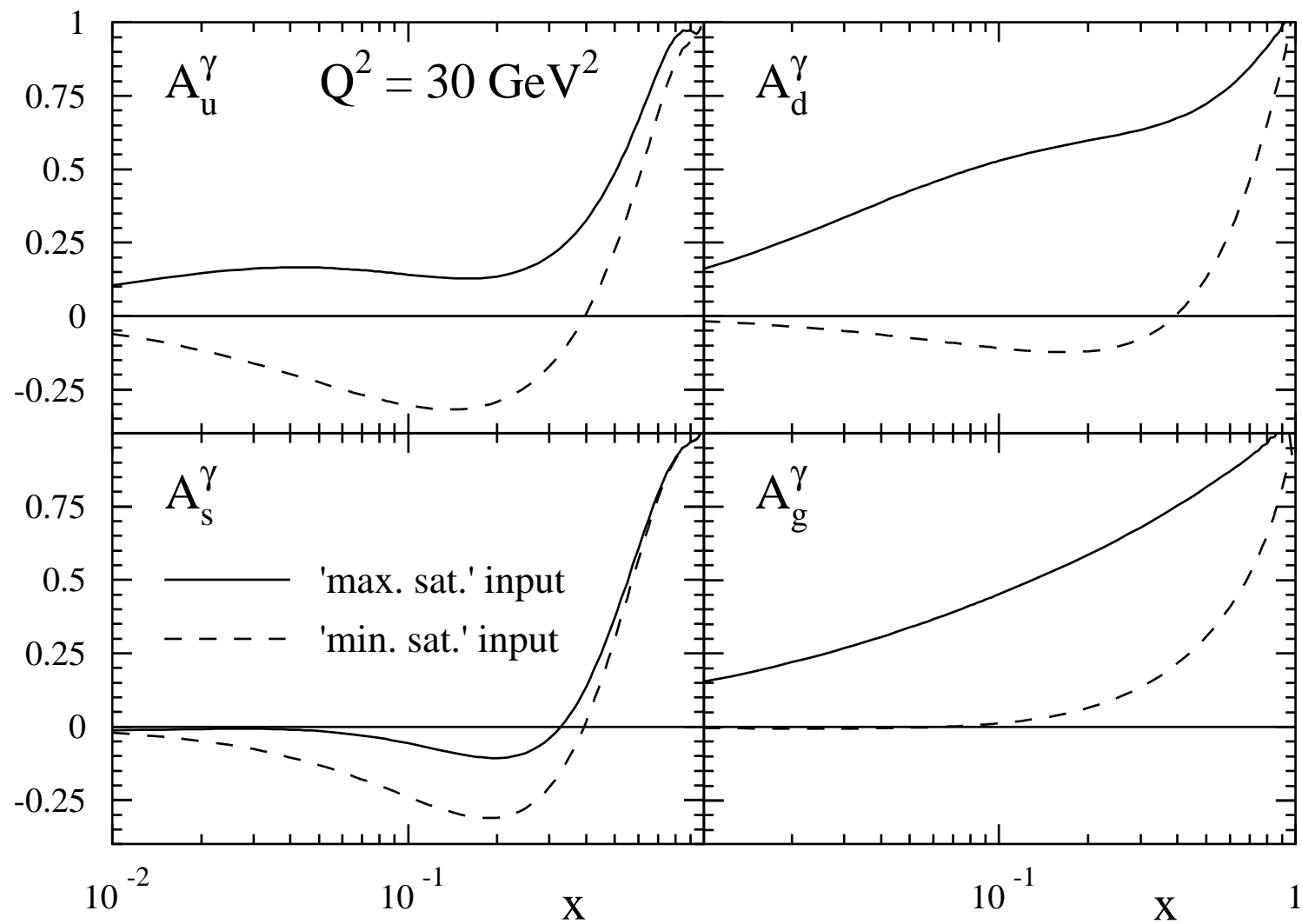


Fig. 2

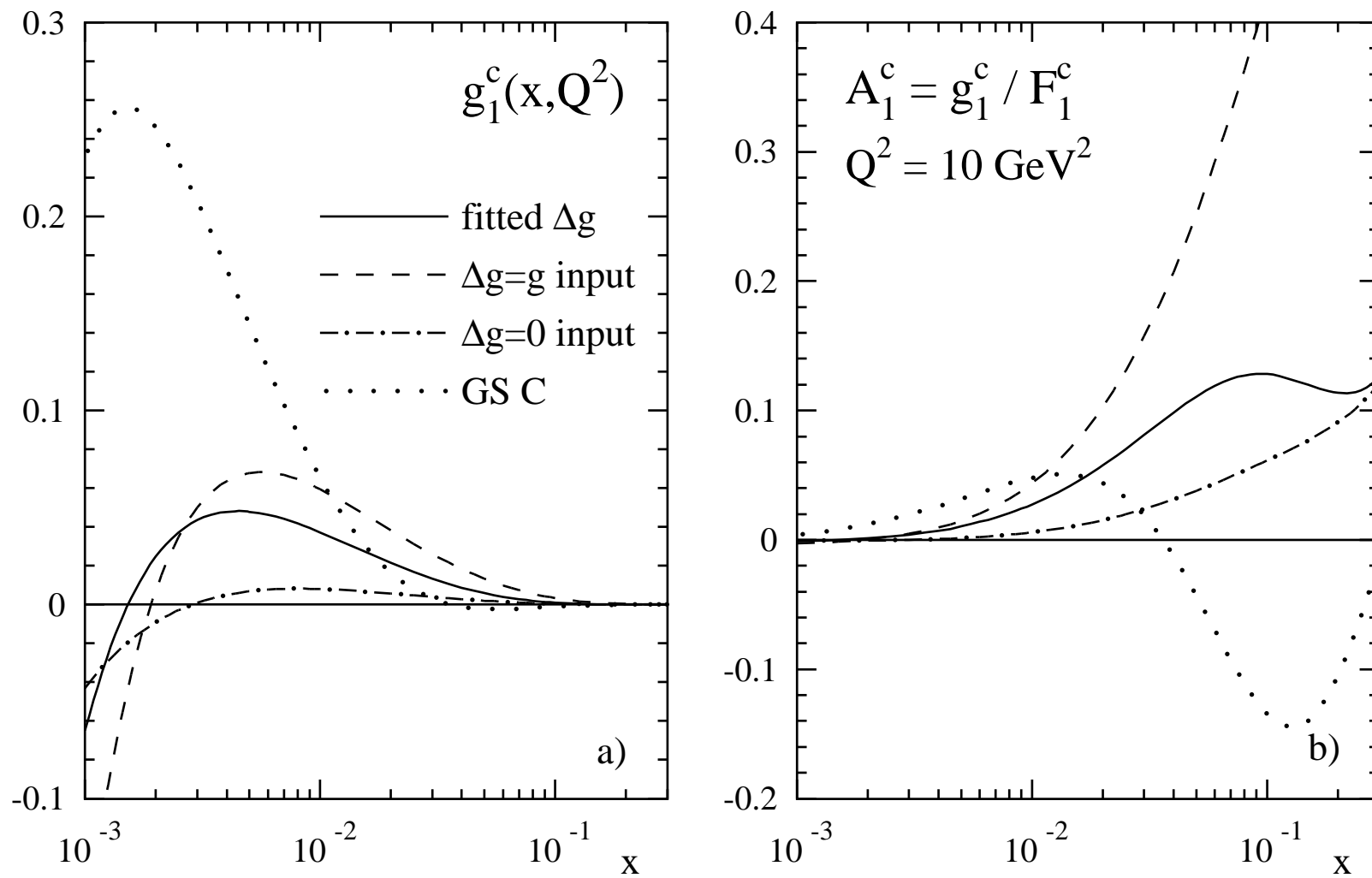


Fig. 3

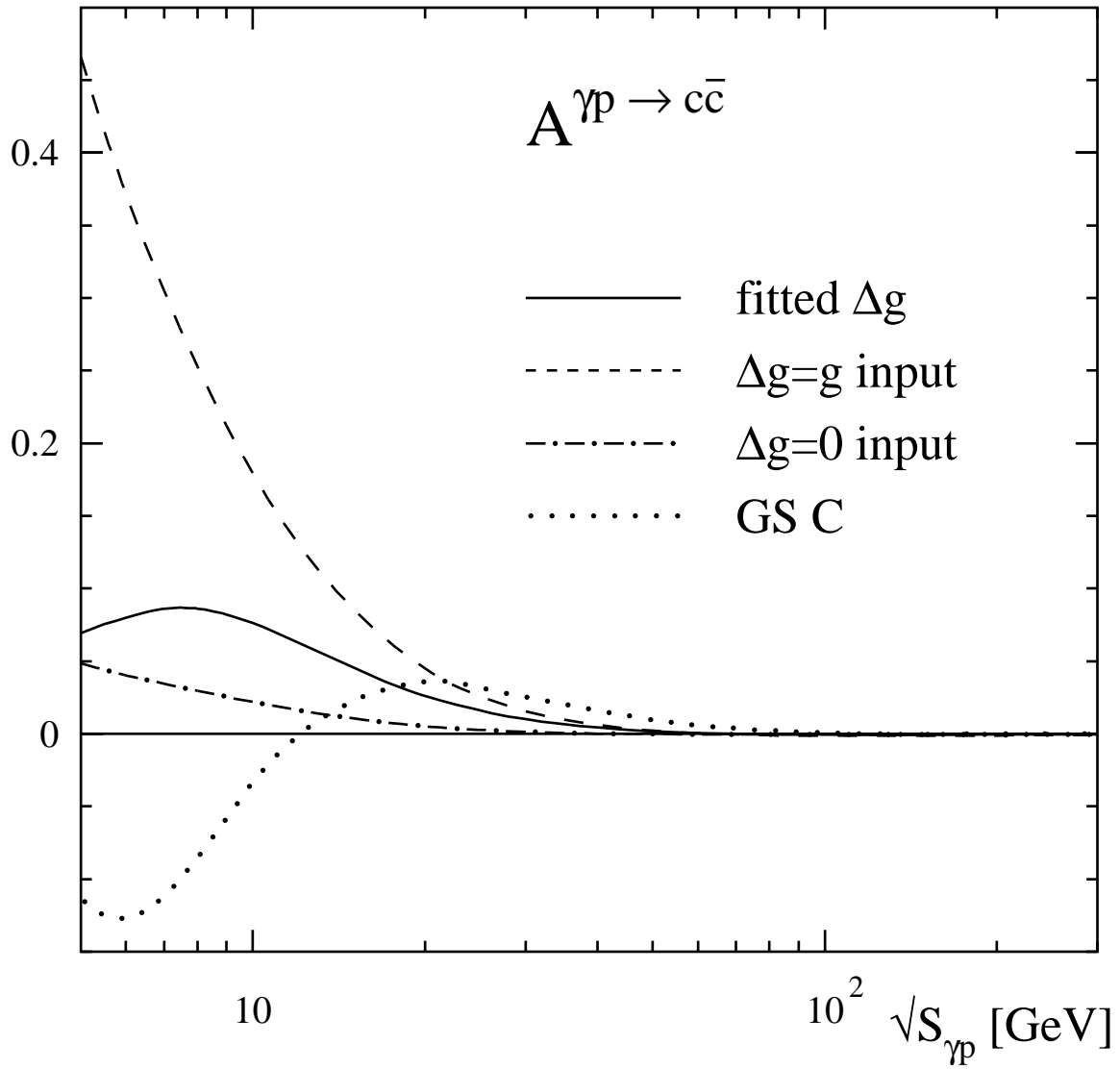


Fig. 4

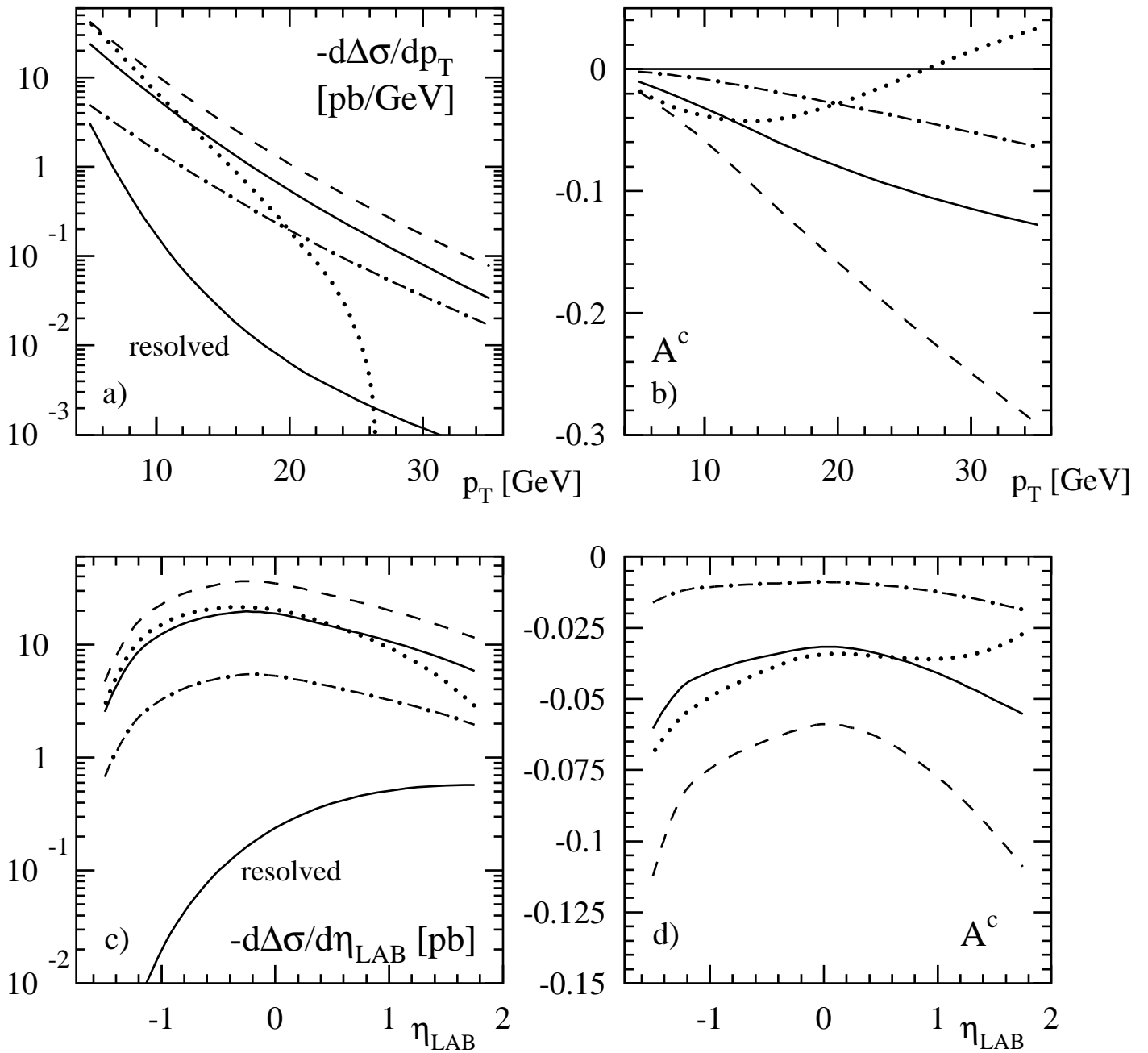


Fig. 5

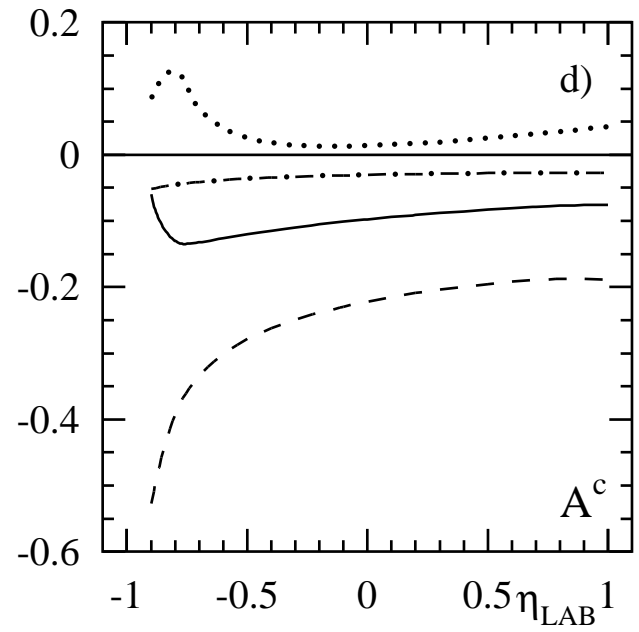
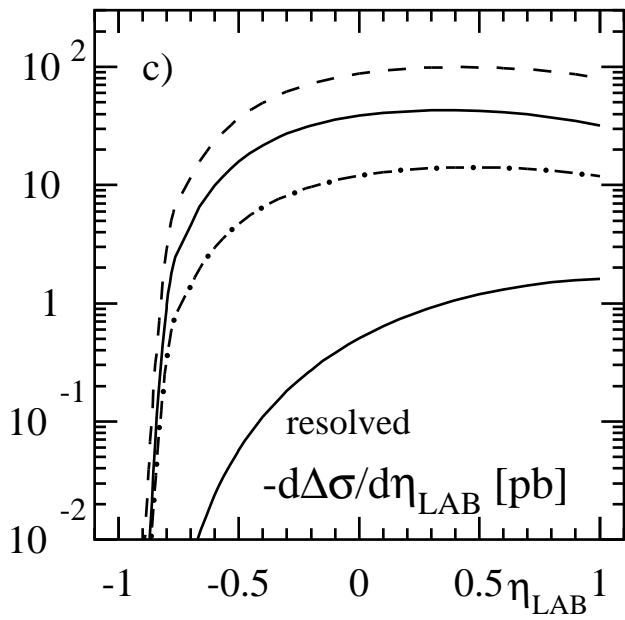
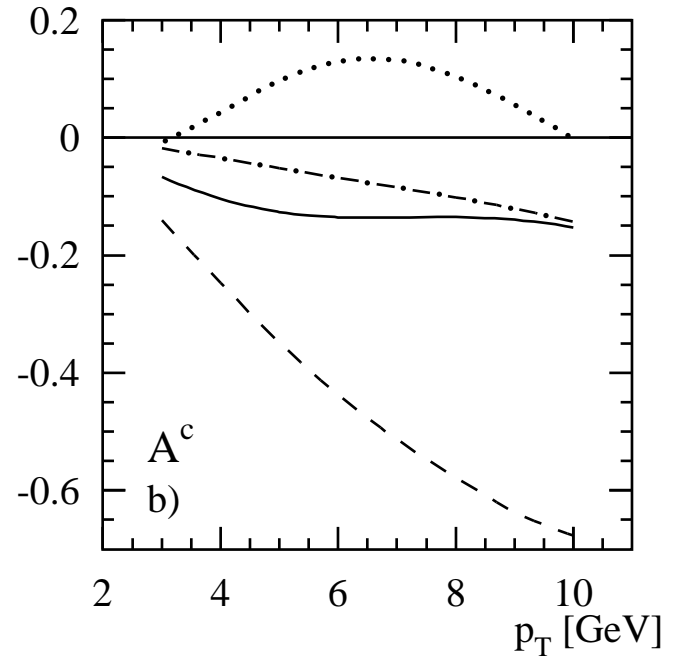
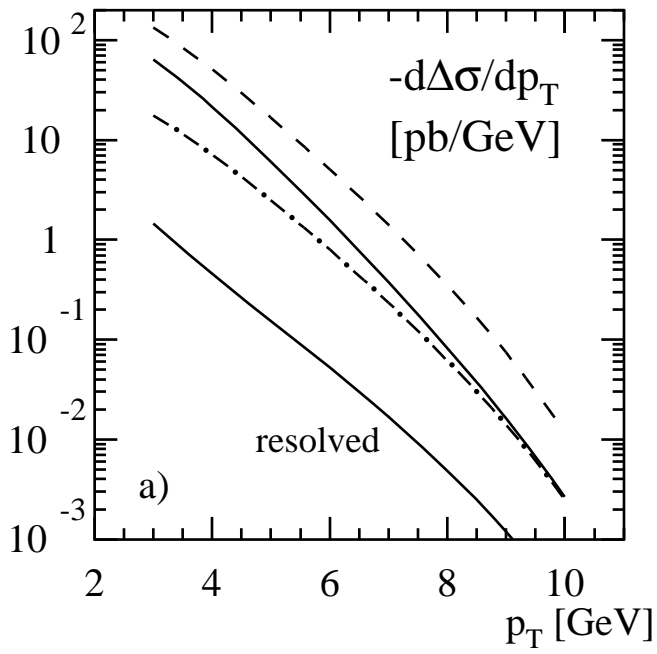


Fig. 6

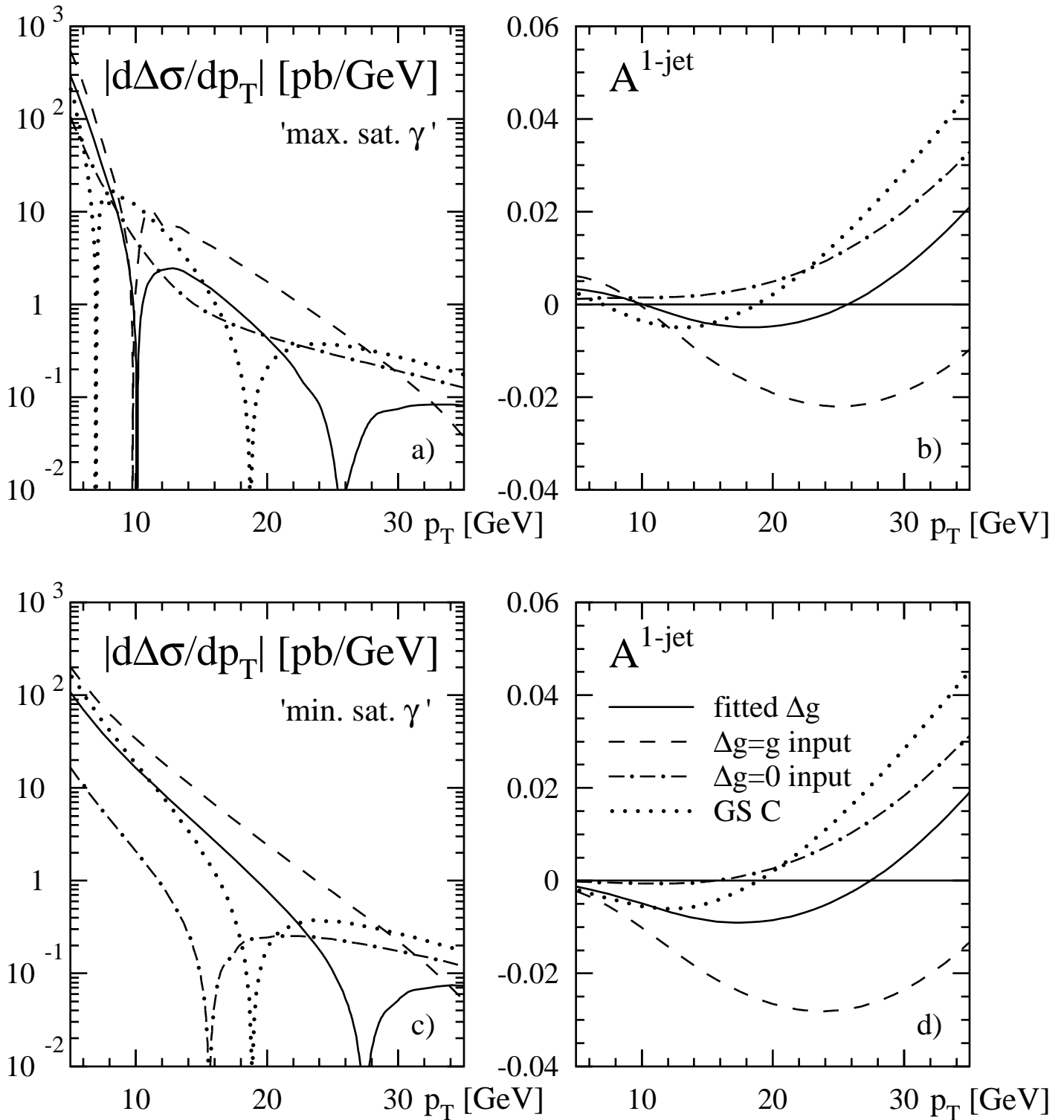


Fig. 7

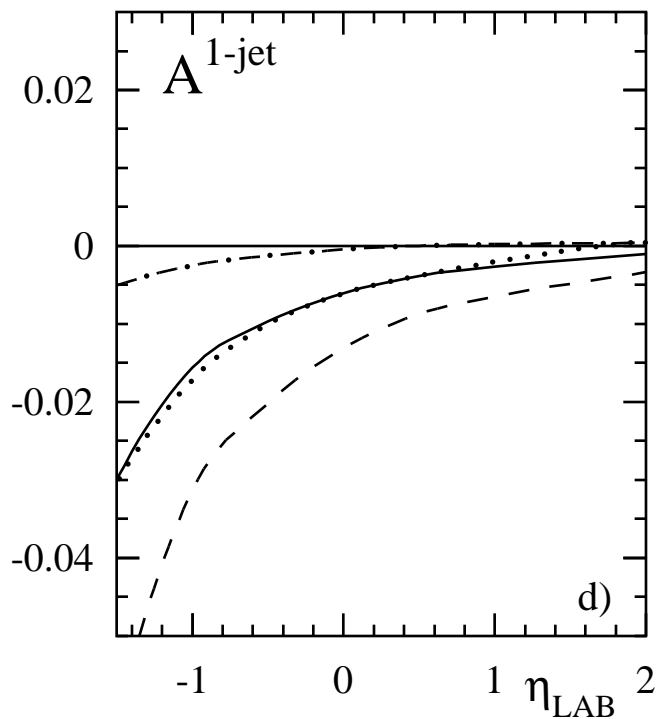
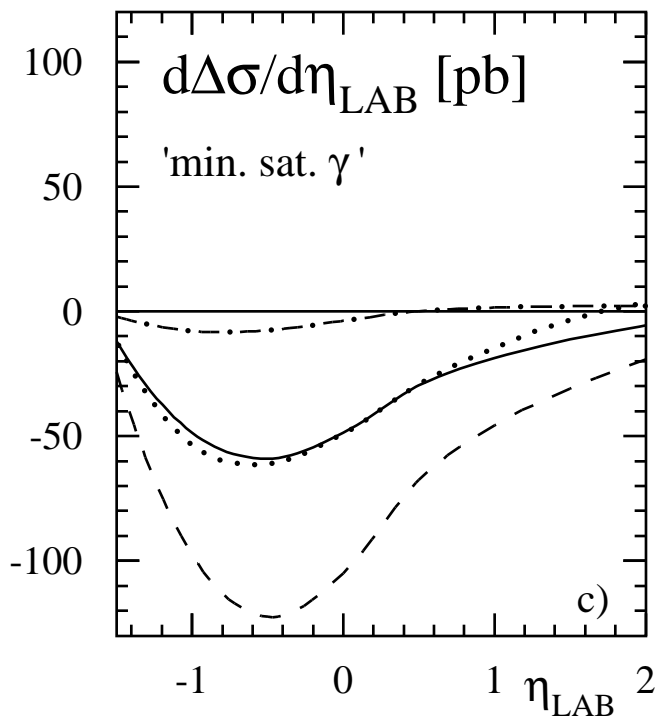
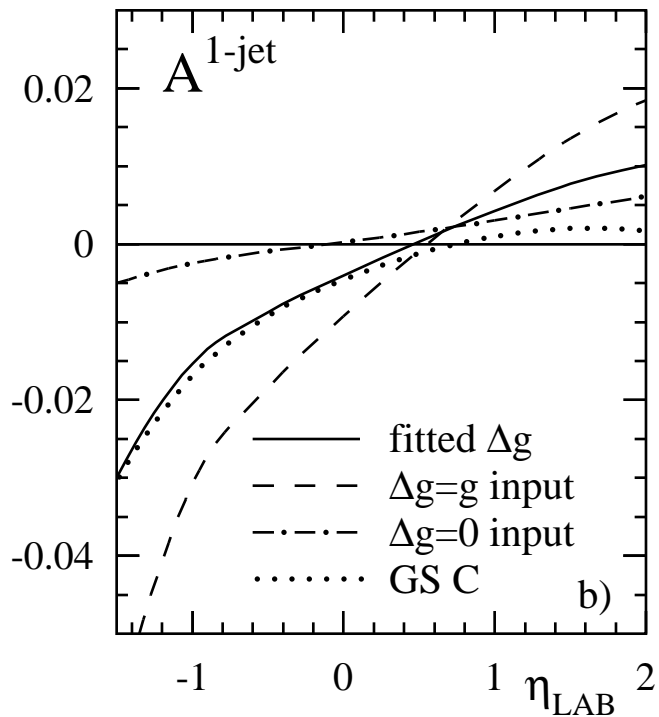
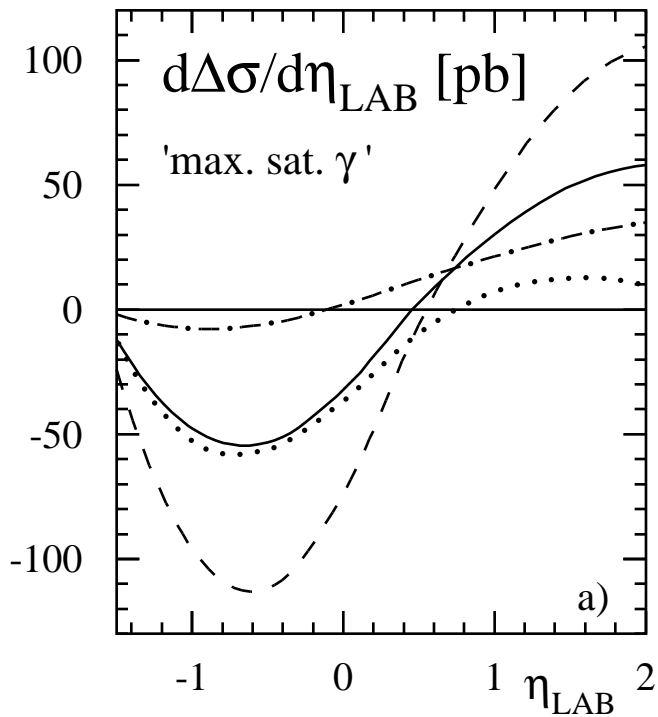


Fig. 8

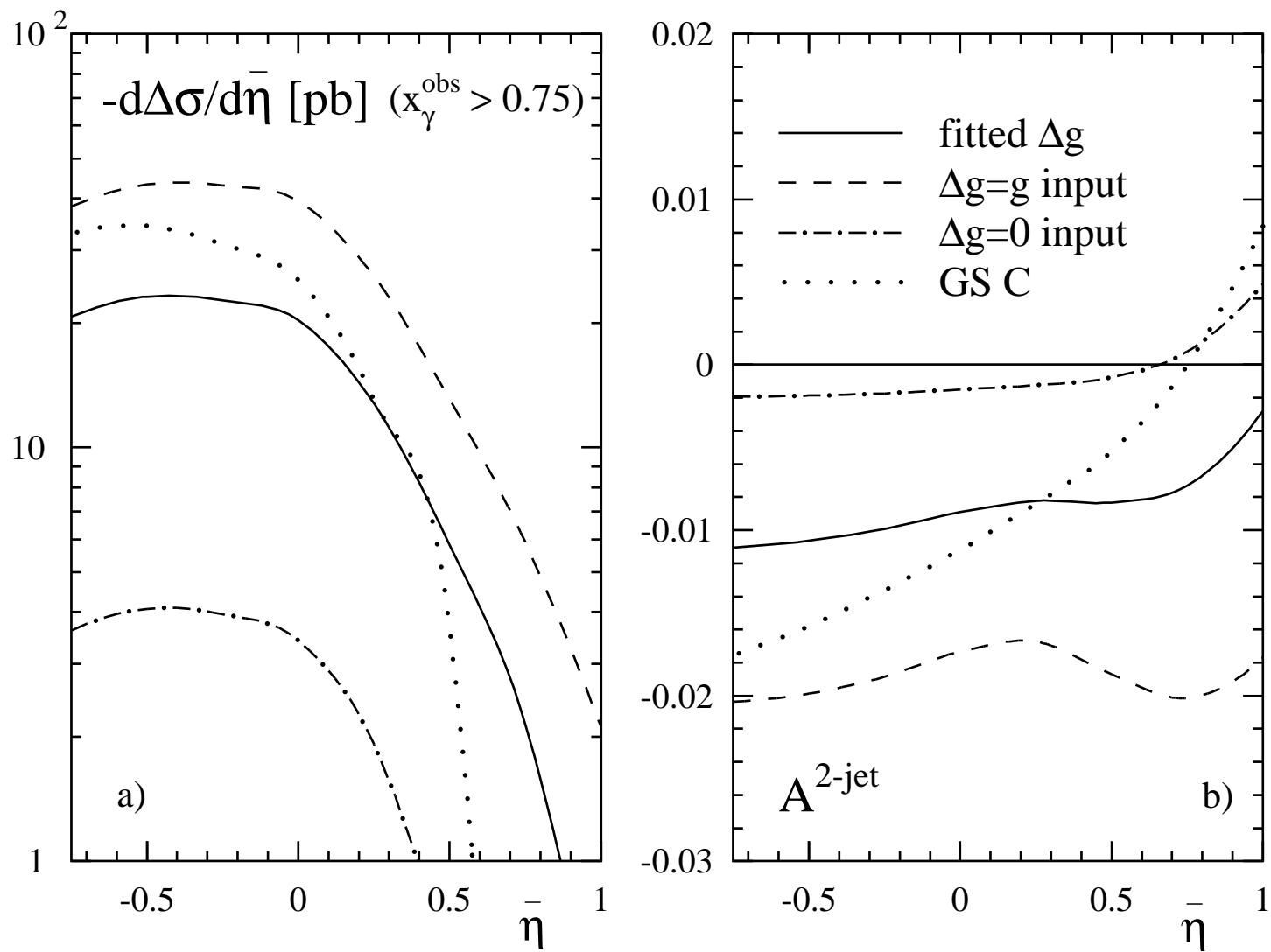


Fig. 9

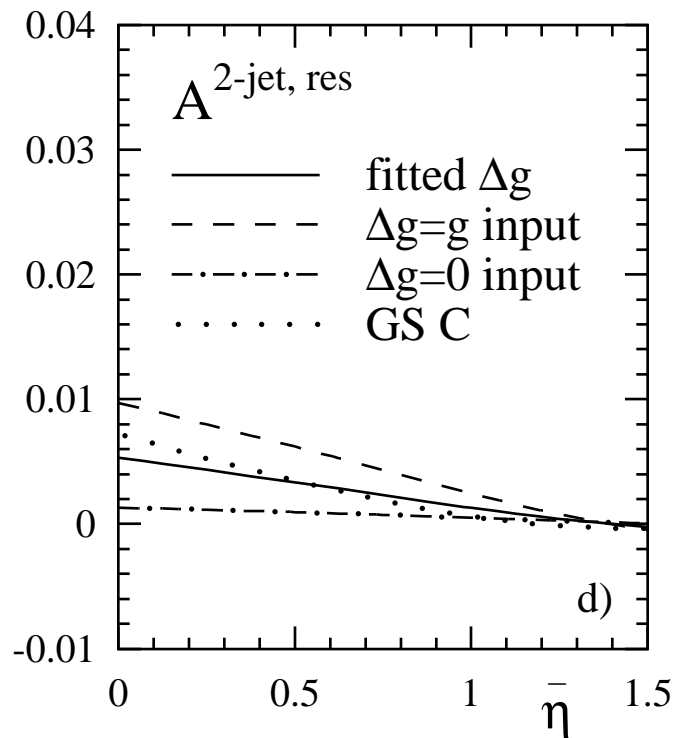
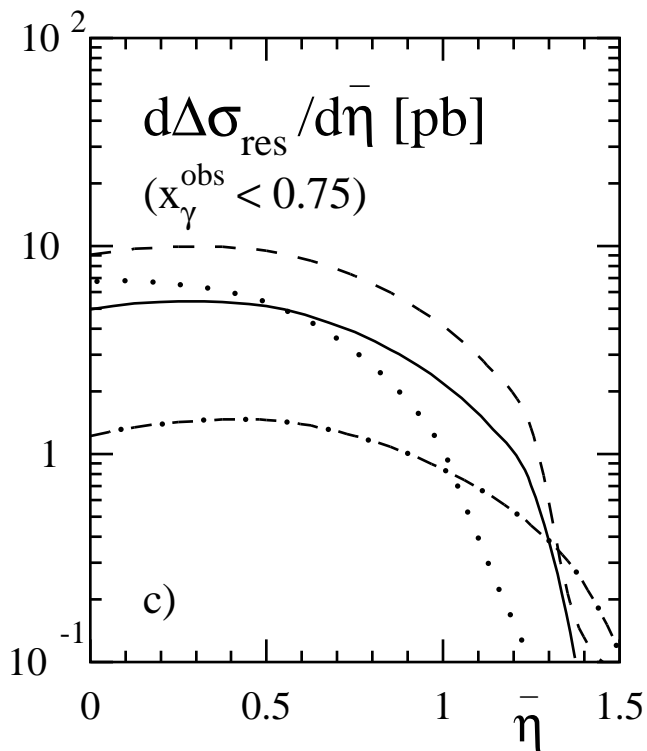
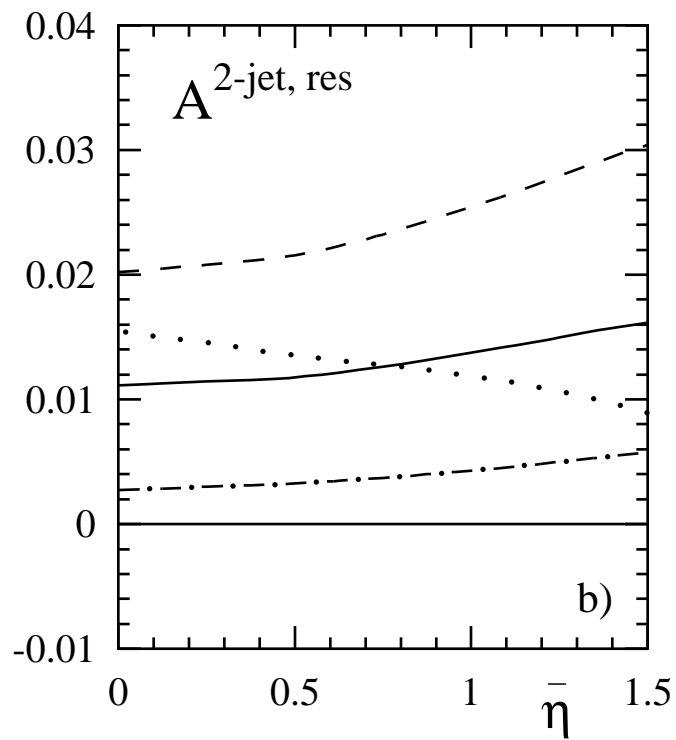
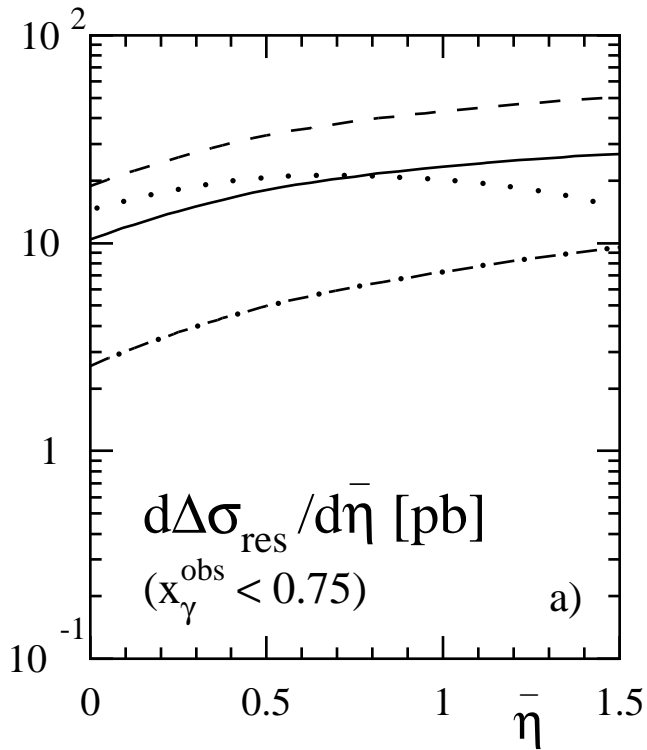


Fig. 10